

## Superamphiphobic surfaces

Zonglin Chu and Stefan Seeger\*

Cite this: DOI: 10.1039/c3cs60415b

Received 15th November 2013

DOI: 10.1039/c3cs60415b

www.rsc.org/csr

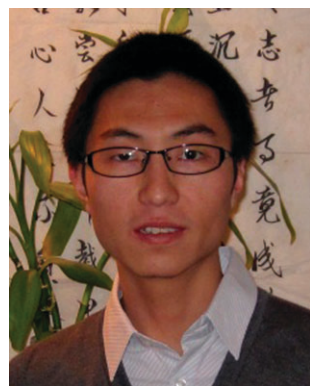
Superamphiphobicity is an effect where surface roughness and surface chemistry combine to generate surfaces which are both superhydrophobic and superoleophobic, *i.e.*, contact angles ( $\theta_{CA}$ ) greater than  $150^\circ$  along with low contact angle hysteresis (CAH) not only towards probing water but also for low-surface-tension 'oils'. In this review, we summarize the research on superamphiphobic surfaces, including the characterization of superamphiphobicity, different techniques towards the fabrication of surface roughness and surface modification with low-surface-energy materials as well as their functional applications.

## 1. Introduction

Research on super-antiwetting and the observation of extremely high  $\theta_{CA}$  dates back to more than a century—a  $\theta_{CA}$  of nearly  $180^\circ$  was firstly achieved *via* coating a substrate with soot, reported by Ollvier in 1907.<sup>1</sup> Thereafter, a super-antiwetting surface with water  $\theta_{CA}$  higher than *ca.*  $150^\circ$  and the sliding angle ( $\theta_{SA}$ ) lower than *ca.*  $10^\circ$ , which is now defined as a

superhydrophobic surface, received continued but relatively limited interest until 1997 when the explanation of the origin and the universal principle of the 'lotus effect' in nature was provided by Barthlott and Neinhuis.<sup>2</sup> They revealed that the epicuticular wax crystalloids on the surface (Fig. 1) are responsible for the superhydrophobicity and self-cleaning properties. Taking the lotus leaf as an example, self-cleaning means that particles adhered to the surface can be removed easily while the droplet is rolling off. Therefore, self-cleaning is a common characteristic of superhydrophobic surfaces. Since then, research interest in superhydrophobicity has been motivated

Department of Chemistry, University of Zurich, Zurich CH-8057, Switzerland.  
E-mail: sseeger@pci.uzh.ch; Fax: +41 (0)44 6356 813; Tel: +41 (0)44 6354 451



Zonglin Chu

Dr Zonglin Chu earned his BSc in Applied Chemistry from Hunan University, China, in 2006, joined Prof. Yujun Feng's group as a Master-to-PhD student at Chengdu Institute of Organic Chemistry, Chinese Academy of Sciences the same year, and received his PhD in Chemical Engineering in 2011. His PhD project in the field of alkylamidodisulfobetaine wormlike micelles and stimuli-responsive worms resulted in more than 10

publications in high impact factor journals. After one year of postdoctoral research in multi-step organic synthesis in the Lab of Organic Chemistry, ETH Zürich, he is currently working on superamphiphobic surfaces in Prof. Dr Stefan Seeger's group in the Department of Chemistry, University of Zurich. His research interests lie at the interface of organic synthesis, colloid and interface science, hydrogels, smart materials, and functional surfaces with special wettability.



Stefan Seeger

Stefan Seeger studied chemistry at the Ruprecht Karl University of Heidelberg and at the Technical University of Berlin. In 1992 he attained a doctorate in chemistry in Heidelberg. Subsequently, Stefan Seeger led the Department of Biophysical Chemistry at the Physico-chemical Institute at the University of Heidelberg, where he was appointed a scientific assistant later. Between 1988 and 1992 he studied marketing and management at the University of Hagen. In 1995 he undertook a six month research stay at the Chemical Center of the University of Lund, Sweden. One year later he attained his habilitation in Heidelberg and in summer 1997 he was appointed as a professor of biochemistry and biosensor technology at the University of Regensburg. In November 1999 Stefan Seeger was appointed as a professor of physical chemistry at the University of Zurich.

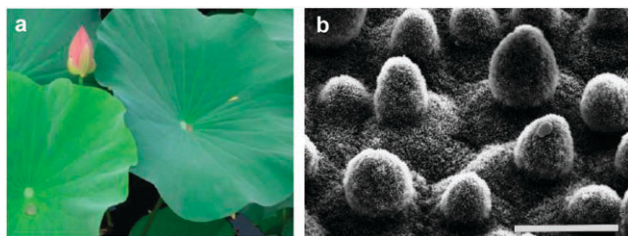


**Fig. 1** Lotus leaves in nature: self-cleaning behaviour (a) and the related microstructures as observed by scanning electron microscopy, SEM (b). Scale bar = 20  $\mu\text{m}$ . (a) Reproduced with permission from ref. 3. (b) Reproduced with permission from ref. 2, Copyright 1997 by Springer-Verlag Berlin/Heidelberg.

by mimicking nature, and thereby great effort was devoted to the understanding of the surface structures of different plants and animals, and therefore the fabrication of similar artificial materials.<sup>3,4</sup>

However, it remains a challenge to create superoleophobic surfaces that resist wetting of organic liquids because of their low surface tension, for example, 23.8  $\text{mN m}^{-1}$  for decane, which is much lower than that of water (72.3  $\text{mN m}^{-1}$ ). To the best of our knowledge, the superoleophobic surface was first developed through the design of re-entrant surface curvature, in conjunction with chemical composition and the roughened texture surface, by Tuteja *et al.* in 2007.<sup>5</sup> Afterwards, it was well-recognized that the combination of appropriate surface roughness and materials with a low surface energy (mainly fluoro-derived compounds) is a successful way to prepare superoleophobic surfaces. Therefore, a variety of superoleophobic surfaces were reported continuously,<sup>6–10</sup> and the terminology ‘superamphiphobic’<sup>6,10</sup> or ‘superomphiphobic’<sup>7</sup> was used to describe the nature of these surfaces—both superhydrophobic and superoleophobic.

This review summarizes the research in this field, describes the analytical methods for superamphiphobicity (Section 2), different techniques towards the fabrication of superamphiphobic surfaces by combining design of surface roughness and surface chemistry (Section 3), and a variety of existing functional applications (Section 4). Finally, a brief overview of the current state and future opportunities in this field is presented.

## 2. Characterization of superamphiphobicity

A sessile drop will normally form in the shape of a sphere sectioned by the surface when it is placed on a flat substrate. There is a discrete and measurable  $\theta_{\text{CA}}$  between the sphere and the surface at the circular solid–liquid–vapour three-phase contact line. Generally, the surface is regarded as hydrophilic when  $\theta_{\text{CA}} < 90^\circ$ ; in other words, the surface is hydrophobic if  $\theta_{\text{CA}} > 90^\circ$ . Specifically, the surface with  $\theta_{\text{CA}} > 150^\circ$ , in addition to a sliding angle  $\theta_{\text{SA}} < 10^\circ$ , is usually named a super-antiwetting (or super-repellant) surface: the surface is deemed as superhydrophobic if the surface displays only water super-repellency; whereas the surface is acknowledged as superamphiphobic if it

exhibits super-repellency towards probing liquids not only water but also low-surface-tension ‘oils’.

The characterization of superamphiphobicity is one of the key issues in the research of superamphiphobic surfaces. The simplest method to characterize a super-repellant surface is eye visualization, in which a gentle flow of a probing liquid is applied to the surface, and the wetting and flowing behaviours are visualized. The surface can be roughly deemed as super-antiwetting if both water and ‘oils’ can move freely on the surface without any sticking. However, to characterize a super-antiwetting surface quantitatively, precise determination of static  $\theta_{\text{CA}}$  and CAH, which is normally performed using commercial instruments, is needed.

### 2.1. Static contact angle

More than 200 years ago, Thomas Young, the genius polymath who made major contributions to vision, physiology, sound, light, language, solid mechanics, and Egyptology, described the forces acting on a liquid droplet spreading on a surface (Fig. 2a). The  $\theta_{\text{CA}}$  of the drop is related to the interfacial energies acting between the solid–liquid ( $\gamma_{\text{SL}}$ ), solid–vapour ( $\gamma_{\text{SV}}$ ) and liquid–vapour ( $\gamma_{\text{LV}}$ ) interfaces following:

$$\cos \theta_{\text{CA}} = \frac{\gamma_{\text{SL}} - \gamma_{\text{SV}}}{\gamma_{\text{LV}}} \quad (1)$$

The above equation known as Young’s equation is a clear oversimplification of the real situation as it is strictly valid only for surfaces that are chemically homogeneous, atomically smooth, and those that do not change their characteristics due to interactions of the probing liquid with the substrate, and any other outside force.<sup>11</sup> Notably, there is absolutely no such ideal surface in the real world. Therefore, two different models, the so-called Wenzel regime<sup>12</sup> (Fig. 2b) and Cassie–Baxter regime<sup>13</sup> (Fig. 2c), were developed to explain the wetting behaviour on a rough surface.

In the Wenzel regime (Fig. 2b), the difference in the measured  $\theta_{\text{CA}}$  from the ‘true’ contact angle of a flat surface ( $\theta_{\text{F}}$ ) is described as follows:

$$\cos \theta_{\text{CA}} = R \frac{\gamma_{\text{SL}} - \gamma_{\text{SV}}}{\gamma_{\text{LV}}} \quad (2)$$

where  $R$  is the ratio of the actual surface area of the rough surface to the apparent area. In this regime, surface roughness can promote either wettability ( $\theta_{\text{CA}} < 90^\circ$ ) or non-wettability ( $\theta_{\text{CA}} > 90^\circ$ ), depending on the chemical properties of the surface.

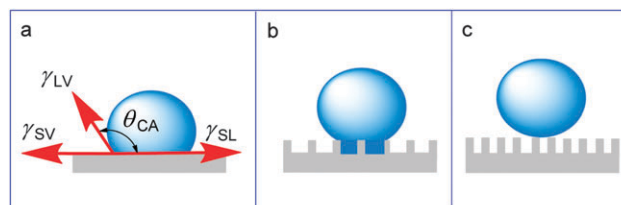


**Fig. 2** Schematic illustration of a droplet placed onto a flat substrate (a) and rough substrates (b) and (c). Depending on the roughness of the surface, the droplet is either in the so-called Wenzel regime (b) or the Cassie–Baxter (c) regime.

1 Interestingly, if the surface is composed of small protrusions  
 2 that cannot be filled by the liquid and are thus filled with  
 3 air (*i.e.*, trapping of air underneath the liquid droplet), the  
 4 wetting phenomenon can be described by the so-called Cassie-  
 5 Baxter regime:

$$\cos \theta_{CA} = -1 + \Phi_S \left( 1 + \frac{\gamma_{SL} - \gamma_{SV}}{\gamma_{LV}} \right) \quad (3)$$

6 where  $\Phi_S$  is the fraction of the surface that is in contact with the  
 7 liquid. In such a case, the liquid touches only the top of the  
 8 surface with very limited contact area. The corresponding  $\theta_{CA}$   
 9 is always much higher than that of a flat surface composed of the  
 10 same material since the pores are filled with air, which is  
 11 hydrophobic. Hence, surface topography plays a very profound  
 12 effect on the wettability.

13 **2.1.1. Contact angle measurements with a sessile drop of  
 14 water.**  $\theta_{CA}$  measurement is one of the most important methods  
 15 for the characterization of a superamphiphobic surface.  
 16 This can be performed on a commercial instrument [for  
 17 example, Contact Angle System OCA (Stuttgart, Germany),  
 18 Krüss DSA Series (Hamburg, Germany), Rame-Hart Goni-  
 19 ometers (Succasunna, USA), and CAM Goniometers (KSV Instru-  
 20 ments Ltd, Helsinki, Finland)] using a charge-coupled device  
 21 camera that is used for recording the image of a water droplet on  
 22 a surface, and analysis software that provides different fitting  
 23 models such as circle fitting, ellipse fitting, tangent searching,  
 24 and Laplace–Young fitting. The calculated  $\theta_{CA}$  may vary a lot for  
 25 the same volume of water droplets (normally 5 to 10  $\mu\text{l}$ ) on the  
 26 same surface when using different fitting models. For example,  
 27 the maximum  $\theta_{CA}$  that can be obtained using circle fitting,  
 28 ellipse fitting, and tangent searching models is around 156°;  
 29 however, the maximum value of around 180° will be obtained  
 30 when Laplace–Young fitting is adopted.<sup>3</sup> This is because the  
 31 deformation of a water droplet caused by the gravity was  
 32 calibrated in Laplace–Young fitting; whereas it was not excluded  
 33 for the other fittings. Therefore, the fitting model should be  
 34 mentioned when reporting data for  $\theta_{CA}$ .

35 In our work,<sup>14</sup> we realized that a good optical presentation of  
 36 the water droplet is crucial to get reproducible  $\theta_{CA}$ . Besides,  
 37 the obtained value can also be affected by the focus of the camera,  
 38 light intensity, contrast of the image, and the settlement of the  
 39 three phase contact baseline, especially when  $\theta_{CA} > 150^\circ$ . For  
 40 example, the apparent value for the same droplet may vary from  
 41 165° to 175° by only a small tuning of the above parameters.  
 42 Therefore,  $\theta_{CA}$  at various positions is normally recorded so as to  
 43 get a more trustable average value.

44 **2.1.2. Contact angle measurements with a sessile drop of a  
 45 low-surface-tension, organic liquid.** Sessile drop measurement  
 46 with water is not sufficient for the characterization of a super-  
 47 amphiphobic surface; in such a case,  $\theta_{CA}$  test with low-surface-  
 48 tension liquids should be performed in addition.<sup>9,15</sup> Such prob-  
 49 ing liquids are mainly non-polar alkanes such as *n*-hexadecane,  
 50 *n*-dodecane, *n*-decane, and cyclohexane,<sup>9,15,16</sup> but polar solvents  
 51 such as toluene, diodomethane,<sup>9</sup> and any other oils (*e.g.*, mineral  
 52 oil and cooking oils) are also frequently used.<sup>9,16</sup> Generally,  $\theta_{CA}$   
 53 of different liquids on the same surface decreases with the

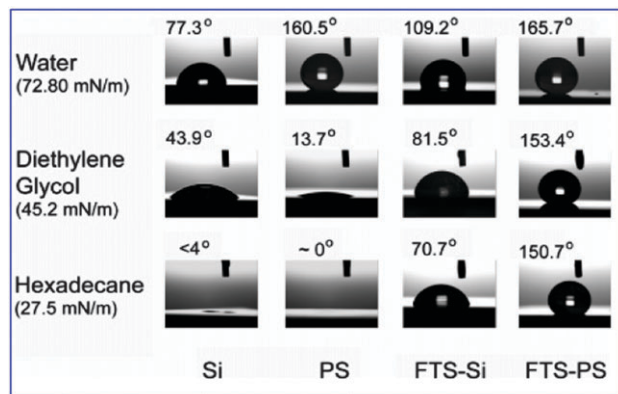


Fig. 3 Static contact angles of water, diethylene glycol, and hexadecane on flat silicon (Si), porous silicon (PS) with tilted pores, flat silicon coated with FTS (FTS-Si), and porous silicon with tilted pores coated with FTS (FTS-PS). Reprinted with permission from ref. 16, ACS Copyright 2008.

increase of the surface tension of the probing liquid (Fig. 3).<sup>16</sup>  
 That's why 'oils' spread quickly on a solely superhydrophobic  
 surface<sup>15</sup> and  $\theta_{CA}$  analysis with 'oils' is needed for the char-  
 acterization of superamphiphobicity.<sup>9,15</sup> As is clearly shown in  
 Fig. 3, flat silicon is both hydrophilic and oleophilic; porous  
 silicon (PS) is superhydrophobic but superoleophilic; 1H,1H,2H,2H-  
 perfluorooctyl trichlorosilane (PFOTS) coated silicon (FTS-Si)  
 is hydrophobic but oleophilic; PFOTS coated porous silicon  
 (FTS-PS) is both superhydrophobic and superoleophobic,  
*i.e.*, superamphiphobic.

## 2.2. Contact angle hysteresis

Whether surfaces displaying  $\theta_{CA} > 150^\circ$  for probing liquids both  
 water and 'oils' are truly superamphiphobic remains unknown  
 if the corresponding CAH is not determined. For example,  
 despite a high  $\theta_{CA}$  (*ca.* 160°) for rapeseed oil on a superhydro-  
 phobic surface composed of surface-fluorinated carbon nano-  
 tubes, the oil droplet remained pinned to the surface when the  
 substrate was tilted.<sup>17</sup>

Any real surface exhibits two contact angles, the so-called  
 advancing contact angle ( $\theta_{Adv}$ ) and the receding contact angle  
 ( $\theta_{Rec}$ ). The difference between them is a presentation of the  
 surface 'non-ideality', and commonly referred to as the CAH,<sup>11</sup>  
 which is intimately related to the adhesion of materials on the  
 surface. Conventionally, superhydrophobicity means not only a  
 high  $\theta_{CA}$  but also a low CAH because the low hysteresis is respon-  
 sible for the self-cleaning behaviour.<sup>3</sup> Therefore, CAH measurement  
 is the other most important method for the characterization of a  
 superamphiphobic surface. Many techniques have been developed  
 to date to characterize the CAH, and amongst them  $\theta_{Adv}/\theta_{Rec}$  and the  
 tilt angle are the most often used ones.

**2.2.1. Advancing/receding contact angle.**  $\theta_{Adv}/\theta_{Rec}$  can be  
 measured using a commercial instrument with an enhanced  
 video microscopy system incorporating digital image analysis,  
 for example, Krüss DSA (Germany). A syringe pump is used to  
 generate a water droplet on the substrate, and to control the  
 rate of water pumping and suction through the needle to

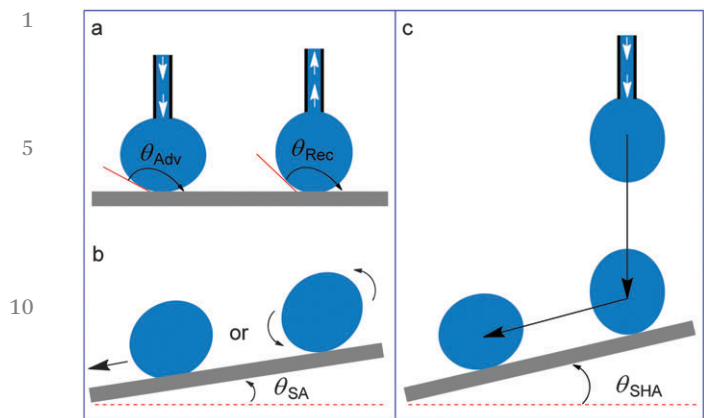


Fig. 4 Schematic illustration of the techniques for the determination of contact angle hysteresis: advancing  $\theta_{Adv}$  and receding contact angle  $\theta_{Rec}$  (a); tilt angle, *i.e.*, the so-called roll off angle or sliding angle  $\theta_{SA}$  (b); and the shedding angle  $\theta_{SHA}$  (c).

perform the advancing and receding, respectively. After the drop-forming step, water is continuously and slowly pumped into (or sucked from) the droplet at a rate smaller than  $0.3 \text{ ml min}^{-1}$  and  $\theta_{Adv}$  was recorded simultaneously by a frame grabber using a solid state charge coupled device camera (Fig. 4a, right). In the last step, the water droplet is receded and  $\theta_{Rec}$  is recorded (Fig. 4a, left).<sup>18</sup>

**2.2.2. Tilt angle.** The tilt angle refers to the critical angle between the substrate and the horizontal surface, below which the droplet starts to move upon elevating one end of the substrate. It should be pointed out that the tilt angle reflects, but not equals to, the difference between  $\theta_{Adv}$  and  $\theta_{Rec}$ .<sup>3</sup> A low tilt angle is crucial to the so-called self-cleaning behaviour, and superamphiphobic surfaces should show a tilt angle lower than  $10^\circ$  for both water and ‘oils’. The tilt angle measurements are of two types—the sliding angle  $\theta_{SA}$  (Fig. 4b) for macroscopically flat surfaces and the shedding angle  $\theta_{SHA}$  (Fig. 4c) for macroscopically rough surfaces.

The sliding angle, also known as the roll-off angle, indicates the angle of inclination of a surface when a droplet completely rolls off the surface due solely to gravity. In experiments, the  $\theta_{CA}$  measuring instrument is equipped with an additional accessory—a tilt plate with a tunable angle between  $0^\circ$  and  $90^\circ$ . The tilt angle is increased continuously from  $0^\circ$  to  $90^\circ$ , and the angle is recorded as  $\theta_{SA}$  while the droplet is sliding away or rolling off the surface.<sup>9,15,19</sup> Strictly speaking, there is a slight difference between sliding and rolling since the way of droplet moving on the tilt surface is not the same (Fig. 4b). In the former case, the surface area of the droplet in contact with the substrate is slightly higher and fixed because of the high adhesion force in between. In contrast, for the latter case, the contacting area and the adhesion in between are slightly lower, and thereby the droplet rolls freely on the surface. Nevertheless, in most cases they are treated equally since the only important thing is the tilt angle where the droplet moves away rather than the moving manner. The only exception is the case of slippery liquid surfaces—liquids on such surfaces slide freely but

unable to roll due to their special surface structure and unique surface chemical component.<sup>20–22</sup>

$\theta_{SA}$  becomes impractical when macroscopically rough substrates such as cotton fabrics and wools are measured.<sup>19</sup> In order to characterize the superhydrophobicity of a macroscopic textile, a new technique named shedding angle was developed recently.<sup>14</sup> In essence, a water droplet of defined volume is released onto the substrate from a defined height. The minimum angle of inclination at which the substrate needs to be tilted for the drop to completely roll or bounce off the substrate is determined (Fig. 4c). Four parameters were controlled: the tilt of the substrate, the needle-to-substrate distance, the relative distance of the impact point to the lower end of the substrate, and the drop volume. More details about the measuring procedure can be seen in ref. 14.

### 3. Fabrication techniques towards superamphiphobicity

In this section, the fabrication techniques towards the superamphiphobic surface will be described and discussed. As is well-known, the combination of appropriate surface roughness and surface chemistry is crucial to the preparation of superhydrophobic surfaces. Therefore, two steps, *i.e.*, the generation of nanoscale roughness and the functionalization with low surface energy materials (mainly fluorinated small molecules or macromolecules), are involved. Depending on the sequence of the above two steps in the preparation process of a superamphiphobic surface, the fabrication strategies can be classified into the following three strategies (Fig. 5): (1) the ‘pre-roughening + post-fluorinating’ technique (Section 3.1); (2) the ‘pre-fluorinating + post-roughening’ technique (Section 3.2); and (3) the generation of surface roughness and surface fluorination occurs in the same step, *i.e.*, one-pot or *in situ* fabrication techniques (Section 3.3). It should be pointed out that some of the so-called superamphiphobic surfaces that are not truly superamphiphobic (because of their relatively high CAH) are included in this section.

#### 3.1. ‘Pre-roughening + post-fluorinating’

The pre-roughening and post-fluorinating methods available to date will be separately discussed in this section because each of them contains a variety of different ways and there are a lot of combinations that may overlap with each other.

##### 3.1.1. Pre-roughening a substrate

**3.1.1.1. Functionalization with nanoparticles (NPs).** Functionalization with nanoparticles represents an important method to generate nanoscale roughness on a substrate. The nanoparticles can be nanosilicas, silicone nanofilaments, carbon nanotubes, carbon nanofibers, and so on.

Nanosilica is a common type of nanomaterial that is inexpensive and frequently used in the fabrication of surface roughness.<sup>23–25</sup> For example, Leng *et al.*<sup>23</sup> functionalized woven fibers with a layer of microscale silica *via in situ* Stöber reaction, followed by further modification with another layer of nanoscale silica *via*

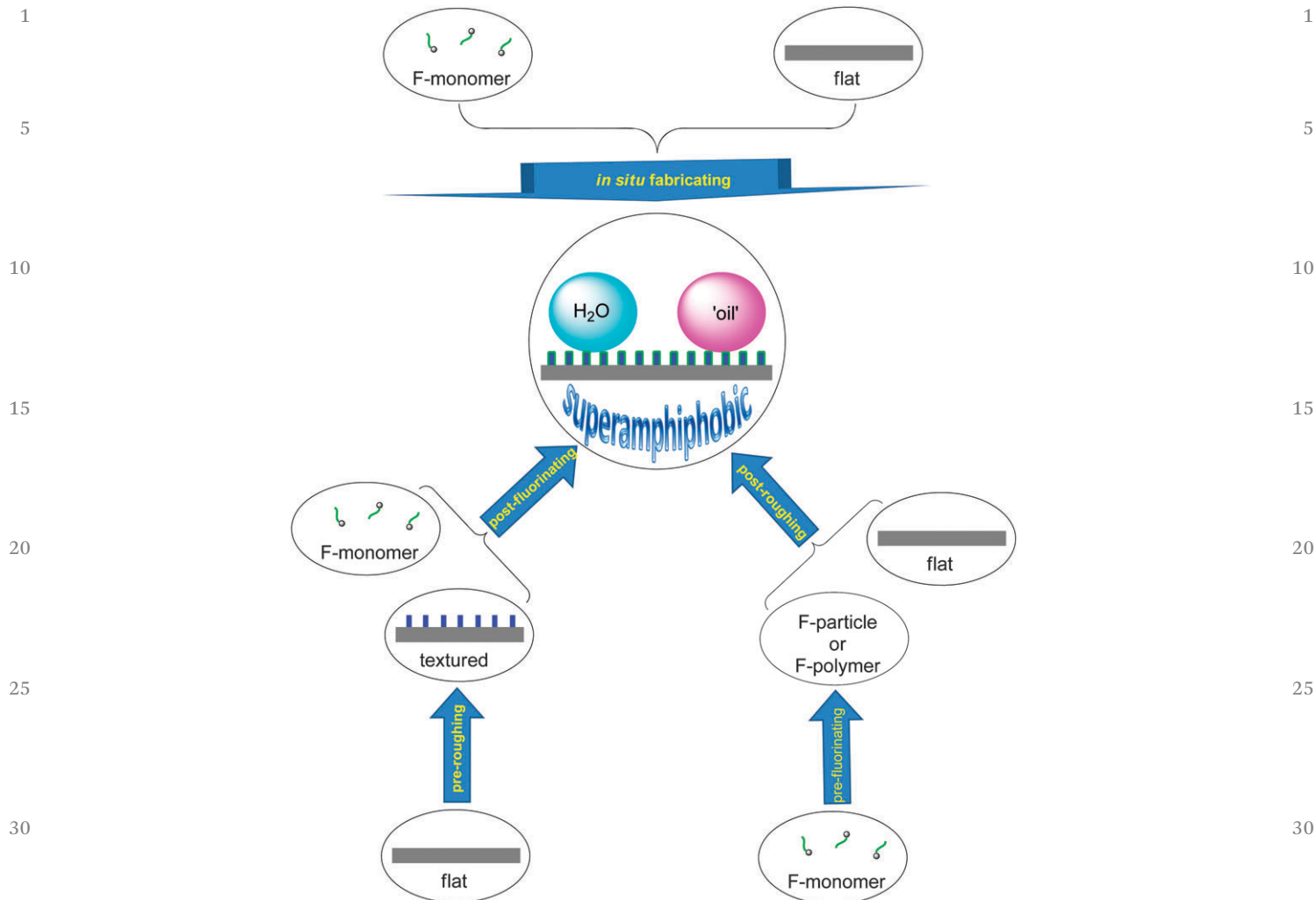


Fig. 5 Three strategies towards the fabrication of superamphiphobic surfaces: pre-roughening + post-fluorination (Section 3.1); pre-fluorination + post-roughening (Section 3.2); and one-pot *in situ* fabrication (Section 3.3).

physical adsorption. Briefly, a piece of cotton textile was immersed in a room temperature mixture of methanol, isopropanol, and ammonium solution in the presence of tetraethylorthosilicate for several hours, and then cleaned with methanol in an ultrasonic bath repeatedly so as to remove the physically adsorbed particles. Subsequently, the obtained textile was soaked in 3-aminopropyltriethoxysiloxane solution to generate surface amine groups which were then protonated with hydrochloric acid. The positively charged textile was then dipped into a suspension of negatively charged nanosilicas, resulting in a layer of silica nanoparticles because of electrostatic attraction. In contrast, Hsieh and coworkers<sup>24</sup> applied hierarchical silica sphere stacking layers to the glass surface *via* the self-assembly technique. It involves a two-stage spin coating of two different silica spheres with a diameter of 20 nm and 300 nm, respectively. A gravitational sedimentation for 2 days made the silica spheres fall onto the surface of the substrate, thus forming well-organized sphere arrays—a closed hexagonal arrangement. A number of large spheres were firstly stacked, followed by the secondary stacking of small silica spheres. He *et al.*<sup>25</sup> spun-coated a mixture

of polydimethylsiloxane (PDMS) and nanosilica onto glass substrates, followed by sintering at 500 °C for 2 h. And the obtained coatings showed higher stability than those just fabricated by spin-coating nanosilica.

For carbon nanotubes (CNTs), numerous applications have been found in many areas of science and engineering because of their excellent electronic, mechanical, and chemical properties. Recently, they were used to create surface roughness so as to impart super-repellant properties to the resultant surfaces.<sup>26,27</sup> For example, Zhang and coworkers<sup>27</sup> demonstrated that the superamphiphobic surface could be obtained as perfluorosilane-rendered TiO<sub>2</sub>/single-walled carbon nanotube composite coatings. Interestingly, the wetting ability of such coatings could be tuned from superoleophobic to superoleophilic *via* ultraviolet irradiation. Moreover, by controlling the dose of UV illumination, superphobicity and superphilicity can exist on the same surface for probing liquids with different surface tensions. Except nanosilica and carbon nanotubes, carbon nanoparticles such as carbon nanofibers,<sup>28</sup> fullerene, graphene as well as other inorganic particles such as nano

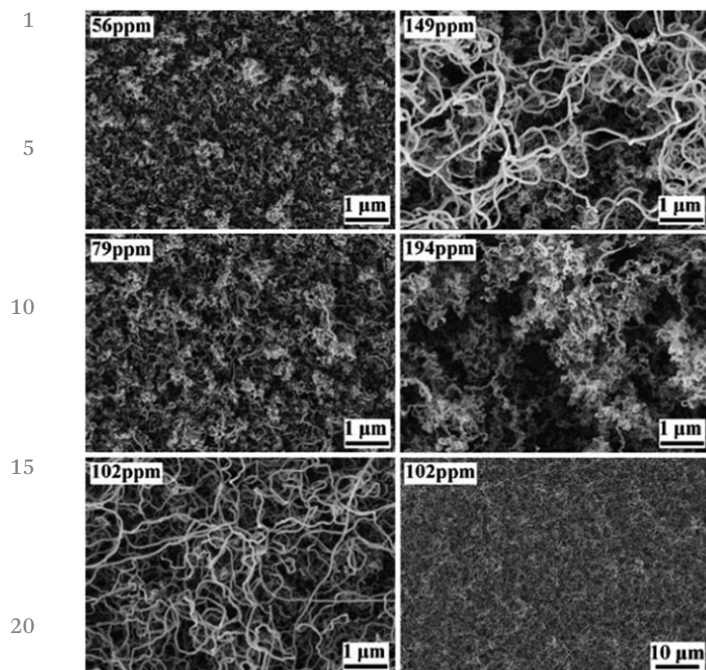


Fig. 6 Surface morphology of the TCMS-coated glass slides at different water concentrations in toluene during the TCMS coating procedure. Scale bars: 1  $\mu\text{m}$ , except for the image at the bottom right corner (10  $\mu\text{m}$ ). Reprinted with permission from ref. 9, Copyright Wiley 2011.

ZnO<sub>2</sub>, CuO, Ca(OH)<sub>2</sub> and CaCO<sub>3</sub> have also been reported to generate surface roughness (see the related references in ref. 25).

Coating a substrate with polyalkylsilsesquioxane filaments (named as silicone nanofilaments, SNF), first reported in 2004, represents an economical and efficient way to prepare a super-repellant surface.<sup>29</sup> Using this technique,<sup>9,14,15,19,29,30</sup> a dense SNF layer can be grown on various substrates, including glass, silicon, ceramics, titanium, aluminium, cotton fabrics, silk, wood, polyethylene, and so on, by either gas<sup>19,30</sup> or liquid (wet toluene)<sup>9</sup> phase deposition of trichloromethylsilane (TCMS) in the presence of a trace amount of water (ca. 50 ppm to 200 ppm)<sup>9</sup> at room temperature (Fig. 6). The as-prepared surface shows extremely water-repellant properties since SNF imparts the surface with not only nanoscale roughness but also low-surface-energy. Besides, such a coating exhibits excellent chemical<sup>31</sup> and environmental stability.<sup>32</sup>

**3.1.1.2. Etching.** Etching<sup>33–41</sup> is a facile and inexpensive method that is frequently used in creating surface roughness. Depending on the nature of the substrate, etching techniques can be classified into the following types: acid etching,<sup>33</sup> base etching,<sup>34,35</sup> electrochemical etching,<sup>36</sup> Au-assisted electrochemical etching,<sup>37</sup> ion etching,<sup>39</sup> plasma etching,<sup>40</sup> and others.<sup>41</sup>

Using engineering metal such as aluminium and its alloys as substrates, Yang *et al.*<sup>33</sup> developed a simple method to achieve hierarchical textured surface morphology by HCl etching and boiling water treatment. Differently, copper substrate can be etched by a base-assist surface oxidation process,<sup>34,35</sup> leaving the surface with hierarchical structure composed of CuO

microflowers and Cu(OH)<sub>2</sub> nanorod arrays.<sup>34</sup> Briefly, copper sheets were immersed in a NaOH solution in the presence of NH<sub>4</sub>S<sub>2</sub>O<sub>8</sub> at room temperature.<sup>34</sup> However, titanium cannot be etched by either acid or base, but can be etched by electrochemical methods. For example, micro-textured Ti can be obtained by electrochemically etching a titanium foil in a dilute NaCl solution at a constant voltage of 15 V for 1 h, as reported by Kim *et al.*<sup>36</sup> Upon further immersing the micro-patterned Ti into a concentrated NaOH solution at 120 °C for 3 h, and subsequently cleaning by dilute HNO<sub>3</sub> and deionized water, TiO<sub>2</sub> nanotube arrays on top of the micro-textured Ti were obtained.

P-type (100) silicon can be roughened *via* an electrochemical etching process. As reported by Cao *et al.*,<sup>37</sup> p-type Si(100) with vertically aligned straight pores was fabricated by anodic etching of Si(100) chips in a Teflon electrochemical cell in the presence of a solution of HF–ethanol and a direct current at a density of 100 mA cm<sup>-2</sup>. In contrast, p-type Si(111) film with tilted pores was fabricated using a gold-assisted electroless etching process.<sup>37</sup> In such a case, the Si(111) film was first coated with Au nanoclusters by dipping in a KAuCl<sub>4</sub>–HF solution; and then it was etched in a Fe(NO<sub>3</sub>)<sub>3</sub>–HF solution at 50 °C, during which the Au nanoclusters served as an electrochemical reaction center. Differently, n-type Si(100) film with surface pyramid structure can be prepared by etching the substrate in an aqueous solution of KOH and isopropanol at 85 °C for 20–30 min.<sup>38</sup> Glass can be tailored by ion etching, and subsequently chemical etching in aqueous HF.<sup>39</sup>

Besides the etching techniques discussed above, other etching methods such as plasma etching<sup>40</sup> and water etching<sup>41</sup> can also be applied, depending on the chemical properties of the substrate.

**3.1.1.3. Lithography.** Lithography is a useful method for fabricating rough surfaces with regular structures. For example, well-defined structures, including pillars with wavy side walls (Fig. 7a),<sup>42</sup> straight smooth side walls (Fig. 7b),<sup>42</sup> and overhang re-entrant structures (Fig. 7c)<sup>42</sup> as well as grooved textures (Fig. 7d)<sup>43</sup> were fabricated by Zhao and coworkers *via* roughening a silicon wafer with a conventional photolithographic technique using a mask, transferring the pattern of the mask to the wafers.<sup>42,43</sup> Similarly, on a large-size template of the transparent PDMS elastomer surface, perfectly ordered microstructures with an inverse-trapezoidal cross section (Fig. 7e) were fabricated by Im *et al.*<sup>44</sup> *via* two consecutive PDMS replication processes and a three-dimensional diffuser lithography technique.

In a recent work reported by Susarrey-Arce and coworkers,<sup>45</sup> arrays of microstructures were successfully fabricated by reactive ion etching of a silicon wafer, which was covered by a patterned photoresist layer. By using the same pitch of a photolithographic mask, the influence of SF<sub>6</sub>, O<sub>2</sub> and CHF<sub>3</sub> gases during the etching process was investigated. Further, it was demonstrated that homogeneous pedestal-like structures can be fabricated by varying the loading conditions during the etching process. The roughness of the microstructures could also be tuned by changing the dry plasma etching conditions.

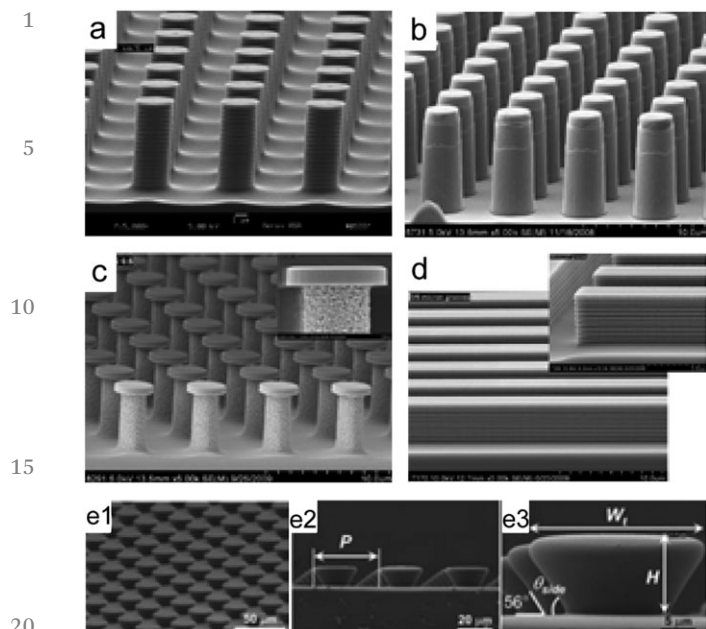


Fig. 7 Well-defined structures prepared *via* Lithography. (a–c) Reprinted with permission from ref. 42, ACS Copyright 2011; (d) reprinted with permission from ref. 43, ACS Copyright 2012; (e) reprinted with permission from ref. 44.

3.1.1.4. *Template-assisted synthesis.* Template assisted synthesis is also frequently employed in fabricating surface roughness.<sup>3</sup>

Deng and coworkers<sup>46</sup> reported a template-assisted synthesis of nanosilica by using candle soot as a template. The deposition of a soot layer was completed by simply exposing a glass slide to the flame of a paraffin candle, which turned the glass black. SEM revealed that the soot consists of a fractal-like network composed of carbon particles with diameters between 30 nm and 40 nm. However, the structure is fragile because the particle–particle interactions are only physical and are weak. When water rolls off the surface, the drop carries soot particles with it, and finally all of the soot deposit can be removed. Inspired by the promising morphology of soot, the authors developed a technique to coat the soot layer with a silica shell, making use of chemical vapor deposition (CVD) of tetraethoxysilane (TES) catalyzed by ammonia. Similar to a Stöber reaction, silica is formed by hydrolysis and condensation of TES. The shell thickness can be tuned by the duration of the CVD process. For example, after 24 h coating, the carbon particles were covered by a 20 nm-thick silica shell. Calcinating the hybrid carbon–silica network at 600 °C for 2 h in air resulted in the combustion of the carbon core and the decrease in the shell thickness, but the surface roughness and network texture could be retained.

In Ganesh *et al.*'s work,<sup>47</sup> a one-dimensional morphology of nanofibers was used as a template to prepare a robust and transparent superamphiphobic coating. The template was fabricated by the deposition of a thick layer of SiO<sub>2</sub> nanofibers on glass. The developed template was subsequently coated with a 25 nm porous silica membrane by vapour phase deposition of triethoxysilane. After 600 °C heat treatment, a transparent,

superhydrophilic coating consisting of a hybrid silica network (branched SiO<sub>2</sub> nanofibers with a surrounding silica membrane) was obtained. It was observed that during annealing, the coated silica membrane reinforced the SiO<sub>2</sub> nanofibers and prevented the fibers from disintegrating into nanoparticles, generating a hybrid silica network. The fiber morphology plays an important role in assisting the hybrid silica network to keep its roughness and surface texture.

3.1.1.5. *Sputter deposition.* Sputter deposition stands for another useful method that can be used for the fabrication of surface roughness. For instance, Fujii *et al.*<sup>48</sup> prepared hierarchical sub-micrometer–nanometer dual pillar surfaces with optimized pillar intervals *via* sputtering Al–Nb alloys onto aluminium substrates, followed by further anodization. In a subsequent work,<sup>49</sup> the authors replaced Al–Nb with Al, and as a result Al was sputter deposited. Nanopores were developed through an anodization process, forming a nanoporous anodic aluminium layer.

3.1.1.6. *Galvanic replacement reaction.* Galvanic replacement reaction is a single step reaction that utilizes the differences in the standard electrode potentials of various metal elements, leading to the deposition of a more noble metal element and the dissolution of a less noble metal element. For example, roughened hierarchical micro/nanostructured Ag deposited layers on Zn substrates were developed *via* galvanic replacement reactions by Zhang and coworkers.<sup>50</sup> Briefly, Zn plates, either those without any pre-treatment or those treated for 2 h in a –20 °C refrigerator or in a 80 °C oven, could be used as the substrates. The galvanic replacement reactions were carried out by simply immersing the substrates in aqueous AgNO<sub>3</sub> for various time intervals, followed by cleaning with deionized water and drying in air. The surface morphology and roughness can be altered through the tuning of the solution concentration, the immersing time, and the pre-treating temperatures.

3.1.1.7. *Sol–gel synthesis.* Sol–gel transition represents another useful technique that can be employed in fabricating surface roughness.<sup>51,52</sup> For example, superoleophobic nanocellulose aerogels have been prepared using unmodified cellulose nanogels, which normally have surface structure with a robust network at several length scales because of the presence of the individual nanofibers as well as their self-assembly aggregates.<sup>51</sup> These gels are usually prepared following a sol–gel transition process. A typical procedure is as follows: a pulp suspension was diluted to 3% consistency firstly, and then the cellulose nanofibers were disintegrated using an ultrafine friction grinder, which consists of a lower and an upper stationary SiC grinding stone with a gap of 100 μm. Water was added during the grinding process, inducing the formation of a nanocellulose hydrogel. Using silica aerogel as a model material, Jin and coworkers<sup>52</sup> prepared superamphiphobic silica aerogel by vapour phase deposition of a fluorinated monomer. Such a surface displays excellent mechanical stability because of its self-similar network structure, which allows fresh re-entrant surface topography even after the removal of the uppermost layer upon mechanical abrasion.

3.1.2. **Post-fluorination of a pre-roughened surface.** After surface roughness is created, the substrates must be further

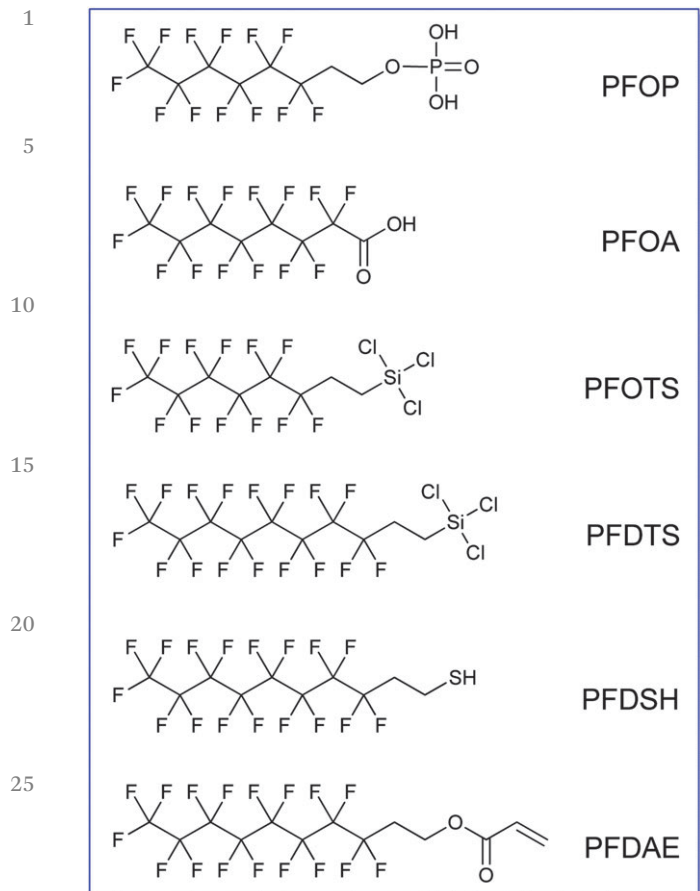


Fig. 8 Chemical structures of functionalized-perfluoroalkanes used in the surface modification of a roughened substrate.

chemically modified with low-surface-energy materials, normally fluorinated compounds, so as to achieve superamphiphobicity. Generally, a fluorinated layer can normally be produced by depositing molecular perfluoroalkane with a functional group at one terminal (F-monomer, Fig. 8), for instance, *1H,1H,2H,2H*-perfluorooctyl phosphate (PFOP),<sup>48,49</sup> *1H,1H,2H,2H*-perfluorooctanoic acid (PFOA),<sup>33,34</sup> *1H,1H,2H,2H*-perfluorooctyl trichlorosilane (PFOTS),<sup>15,36–40,42–47,51</sup> *1H,1H,2H,2H*-perfluorodecyl trichlorosilane (PFDTS),<sup>9,27,41</sup> *1H,1H,2H,2H*-perfluorodecane-1-thiol (PFDSH),<sup>35,50</sup> and *1H,1H,2H,2H*-perfluorodecyl acrylate (PFDAE).<sup>53</sup> However, it can also be achieved by spin-coating a fluorinated-polymer (F-polymer) solution. While grafting a fluorinated layer by using F-monomers, the process can be carried out *via* either vapour<sup>39,42–47,51</sup> or liquid<sup>33–38,40–41,48–50</sup> phase deposition.

### 3.2. 'Pre-fluorinating + post-roughening'

Different from the methods discussed in Section 3.1, "pre-fluorinating + post-roughening" represents another strategy to fabricate a superamphiphobic surface. In such a case, fluorinated polymers or nanoparticles were synthesized firstly, and subsequently applied to flat surfaces *via* spin-coating, spray-coating, dip-coating, electrospinning, sol-gel transition, or other physical techniques, generating roughened structures

with a low-surface-energy layer on the surface. This section is organized according to the different techniques and chemical components that are frequently used for the surface modification of a flat surface.

#### 3.2.1. Spinning or spraying fluorinated silica nanoparticles.

Sheen *et al.*<sup>54</sup> reported a method to prepare fluorinated silica nanoparticles (FSN). Briefly, ammonium hydroxide was added to a mixture of tetraethoxysilane (TEOS) and isopropanol, and the reaction mixture was refluxed at 60 °C so as to induce the growth of silica nanoparticles *via* sol-gel transition. Finally, PFDTS was introduced to terminate the reaction until the sol-gel process was running for 100 min, leaving the silica nanoparticles with an outer fluorinated layer. The substrates (glass slides) after being spin-coated using these fluorinated silica nanoparticles become superamphiphobic with  $\theta_{CA}$  higher than *ca.* 150° for both water and a variety of 'oils'.

Similarly, Campos and coworkers<sup>55</sup> prepared FSN by fluoroalkyl-functionalizing commercial nanosilicas also using PFDTS. These functionalized nanosilicas were dispersed in a mixture of 5 mg ml<sup>-1</sup> commercial fluoropolymer Viton ETP-600S (DuPont) in 1,3-dichloro-1,2,2,3,3-pentafluoropropane, forming a suspension with silica concentration ranging from 0% to 80% (w/w). The fresh FSN suspension was spray-coated onto silicon wafers through an airbrush with a 1.06 mm diameter tip using compressed air, which was repeatedly passed over the substrates laterally at a distance of *ca.* 15–20 cm. Finally, the samples were air-dried for 1 h, followed by further drying at 60 °C for 12 hours. The as-prepared surfaces showed superhydrophobicity when FFNS concentration is higher than 20% (w/w). To achieve superoleophobicity for probing liquid of CH<sub>2</sub>I<sub>2</sub> and rapeseed oil, FFNS concentration of 40% and 70% is needed, respectively. While FFNS concentration equals 80%, the surface exhibited  $\theta_{CA}$  about 160° for hexadecane; however, the corresponding  $\theta_{SA}$  is much higher than 20° due to the extremely low surface tension of hexadecane ( $\gamma_{LV} = 27.5$  mN m<sup>-1</sup>).

#### 3.2.2. Spraying fluorinated carbon nanotubes.

Wang and coworkers<sup>56</sup> synthesized fluorinated multi-wall carbon nanotubes (MWCNTs-PFOL) by grafting *1H,1H,2H,2H*-perfluorodecanol (PFOL) onto multi-wall carbon nanotubes (MWCNTs). Then a nanocomposite containing polyurethane pre-polymers, PFOL, hexanediol, a mixture of acetone and toluene and MWCNTs-PFOL was spray-casted onto a glass slide. The obtained coating shows coralline-like structure (Fig. 9a) and displays  $\theta_{CA}$  greater than 150° for probing liquids not only water but also 'oils' (Fig. 9b). The CAH is low for water ( $\theta_{SA} = 5^\circ$ ) but slightly higher for low-surface-tension oils such as surfactant solution ( $\theta_{SA} = 15^\circ$ ), glycerol ( $\theta_{SA} = 10^\circ$ ), CH<sub>2</sub>I<sub>2</sub> ( $\theta_{SA} = 30^\circ$ ), rapeseed oil ( $\theta_{SA} = 35^\circ$ ), and hexadecane ( $\theta_{SA} = 40^\circ$ ).

#### 3.2.3. Spraying a copper perfluorooctanoate suspension.

Yang *et al.*<sup>57</sup> reported a simple method to prepare copper perfluorooctanoate by reacting copper acetate with perfluorooctanoic acid in aqueous media. Uniform coatings with robust superoleophobicity were produced by spraying the copper perfluorooctanoate suspension onto various substrates. Such coatings displayed apparent  $\theta_{CA}$  greater than 150° and low sliding angles, even with liquids possessing a significantly

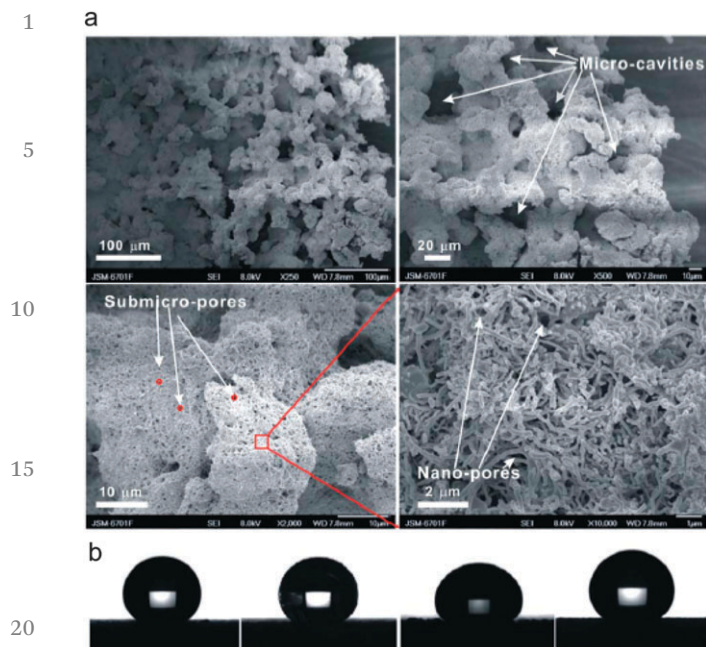


Fig. 9 SEM images of the surface morphology of perfluoroalkyl grafted MWCNTs-PU nanocomposite coatings at different magnifications (a): multi-scale structure with numerous micro-cavities, micro- and nano-pores are formed; and profile images of liquids: water, glycerol,  $\text{CH}_2\text{Cl}_2$ , and hexadecane from left to right (b). Reprinted with permission from ref. 56.

lower surface tension, such as hexadecane and dodecane. The robust superoleophobicity was ascribed to the re-entrant morphology and extremely low surface energy, which can effectively prevent the transition from the Cassie-Baxter state to the Wenzel state. Such a facile technique shows great potential for a wide range of applications because it can be applied to a variety of substrates without limitations of size and shape, do not typically require complicated application methods and can be easily repaired after being mechanically damaged.

### 3.2.4. Electrospinning or spraying a blend of a fluoroalkyl polyhedral oligomeric silsesquioxane and a common polymer.

Electrospinning is a versatile technique for producing micro/nanofibers from a variety of polymers.<sup>58</sup> In a laboratory environment, it requires a high-power supply, a syringe pump, a conducting substrate, and a polymer with high molecular weight as a starting material. The electrospinning process is initiated by a high electric field between the syringe that contains viscous polymer solution and the conducting substrate. A charged liquid jet is ejected from the tip of a distorted droplet because of the high electrical potential. The liquid jet experiences whipping and bending instabilities within a sufficient distance to evaporate its solvent thoroughly and, consequently, becomes a solid micro/nanofiber membrane on the substrate. Recently, superamphiphobic surfaces have been fabricated by electrospinning a blend of a fluorinated polymer and a common polymer.<sup>5,7</sup>

Tuteja and coworkers<sup>5</sup> synthesized a class of hydrophobic polyhedral oligomeric silsesquioxane (POSS) molecules in which the rigid silsesquioxane cage is surrounded by 1*H*,1*H*,2*H*,2*H*-perfluorodecyl or 1*H*,1*H*,2*H*,2*H*-perfluorooctyl

groups (referred to as FD-POSS and FO-POSS, respectively). The high surface concentration and surface mobility of  $-\text{CF}_2-$  and  $-\text{CF}_3$  groups, along with the high ratio of  $-\text{CF}_3/-\text{CF}_2-$ , result in a strongly hydrophobic material with low-surface-energy. A spin-coated film on a flat Si wafer, which had a root mean square roughness of 3.5 nm, exhibited  $\theta_{\text{Adv}}$  and  $\theta_{\text{Rec}}$  about  $124.5 \pm 1.2^\circ$  for probing liquid of water. Surprisingly, rough structure composed of beads-on-strings fibers displaying superhydrophobicity and extremely oleophobicity (but not superoleophobicity) was prepared by electrospinning a 5% (w/w) blend of FD-POSS-poly(methyl-methacrylate) (PMMA) when FD-POSS mass fraction is higher than  $\sim 0.1$ , though the corresponding spin-coated surfaces are oleophilic. It was demonstrated that the local surface curvature plays a key role in driving the oleophobicity, and the electrospinning coating technique can also be applied to fragile or natural substrates so as to confer oleophobicity in addition to superhydrophobicity. In a subsequent work,<sup>7</sup> the authors extended their work by developing four dimensionless design parameters that describe the robustness of a composite interface and the observed apparent  $\theta_{\text{CA}}$  on a textured surface, given the various thermo-physical and geometric properties that parameterize the system. Guided by the design parameters, they developed families of superamphiphobic surfaces by systematically varying the various chemical and topological surface features. Beads-only, beads-on-strings, and fiber-only structures are formed at a solute concentration of 2%, 5%, and 10% (w/w), respectively. Interestingly,  $\theta_{\text{Adv}}$ ,  $\theta_{\text{Rec}}$ , and  $\theta_{\text{SA}}$  for hexadecane on the beads-only surface are  $156^\circ$ ,  $150^\circ$  and  $5^\circ$ , respectively. In comparison, the beads-on-strings and fibers-only surfaces show a slightly higher CAH with  $\theta_{\text{Adv}}/\theta_{\text{Rec}}$  values of  $153^\circ/141^\circ$  and  $153^\circ/134^\circ$ , respectively. Recently, the same research group demonstrated that similar textured surfaces can also be fabricated by spraying the FD-POSS-PMMA blend.<sup>59</sup> Very recently, Pan *et al.*<sup>60</sup> employed an electrospun coating of cross-linked poly(dimethylsiloxane) + 50% FD-POSS (w/w) on top of stainless steel wire meshes to fabricate hierarchically structured surfaces. Such a surface possesses re-entrant curvature at both the coarser length scale and the finer length scale. The hierarchical texture along with the re-entrant curvature and the low surface energy of the coating resulted in a superamphiphobic surface with extremely high  $\theta_{\text{CA}}$  and low CAH for a range of different polar and non-polar low surface tension Newtonian liquids, including various acids, bases, and solvents.

Opposite to the procedures discussed above,<sup>5,7,59,60</sup> by dissolving FD-POSS in a low-molecular-weight fluorinated compound, 1*H*,1*H*,2*H*,2*H*-perfluorobutyl triethoxysilane, Lin *et al.*<sup>61</sup> prepared a viscous solution, which was then dispersed in ethanol. Upon ultrasonication for 0.5 h, a stable, homogeneous suspension was obtained. Such a dispersion can be easily applied onto fabrics so as to impart superamphiphobicity to the surface through a wet-chemical coating technique such as spraying, dip-coating, or padding.

**3.2.5. Coaxial electrospinning a fluorinated polymer and a common polymer.** In contrast to electrospinning, coaxial electrospinning expands the versatility of electrospinning by

enabling the formation of core–sheath-structured micro/nano-fibers. A coaxial nozzle consists of a central tube surrounded by a concentric annular tube. As reported by Steckl *et al.*,<sup>58</sup> a fluoropolymer Teflon AF2400 solution and a common polymer poly( $\epsilon$ -caprolactone) was used as sheath and core material, respectively. Both solutions were separately fed into the coaxial nozzle from which they were ejected simultaneously. A compound pendant droplet was generated from the coaxial nozzle without bias; upon application of a sufficient voltage, a Taylor cone was formed and a liquid jet was ejected that consists of the core material enveloped by the sheath material. Then the polymer jet underwent the same process as in conventional electrospinning; being pulled by the electric field and whipped and stretched by the bending instability, followed by evaporation of the solvent causing the formation of solid-state fibers. The coaxial electrospinning technique allows the resultant fibers to combine different characteristics of both the core and the sheath polymers.

**3.2.6. Sol–gel transition of a fluoropolymer.** In the work by Xiong *et al.*,<sup>62</sup> a diblock copolymer, poly[3-(triisopropoxysilyl)propylmethacrylate]-*block*-poly[2-(perfluorooctyl)ethyl methacrylate], which contains a fluorinated block and a sol–gel forming block, was synthesized by sequential anionic polymerization firstly. And then the diblock copolymer was chemically grafted onto silica particles by inducing sol–gel transition of the poly[3-(triisopropoxysilyl)propylmethacrylate] block using  $\alpha,\alpha,\alpha$ -trifluorotoluene–tetrahydrofuran mixture as a solvent and HCl as a catalyst, generating a polymer monolayer on the surface of silica particles at sufficiently high P1-to-silica mass feed ratios. Finally, the polymer–silica composite was cast-coated onto glass slides and printing paper, leaving the substrate surface with rugged polymer–silica films, which were superamphiphobic.

### 3.3. One-pot methods

Compared with the two strategies discussed above, *in situ* synthesis stands for a simpler way to fabricate superamphiphobic surfaces, and thus was also frequently reported.

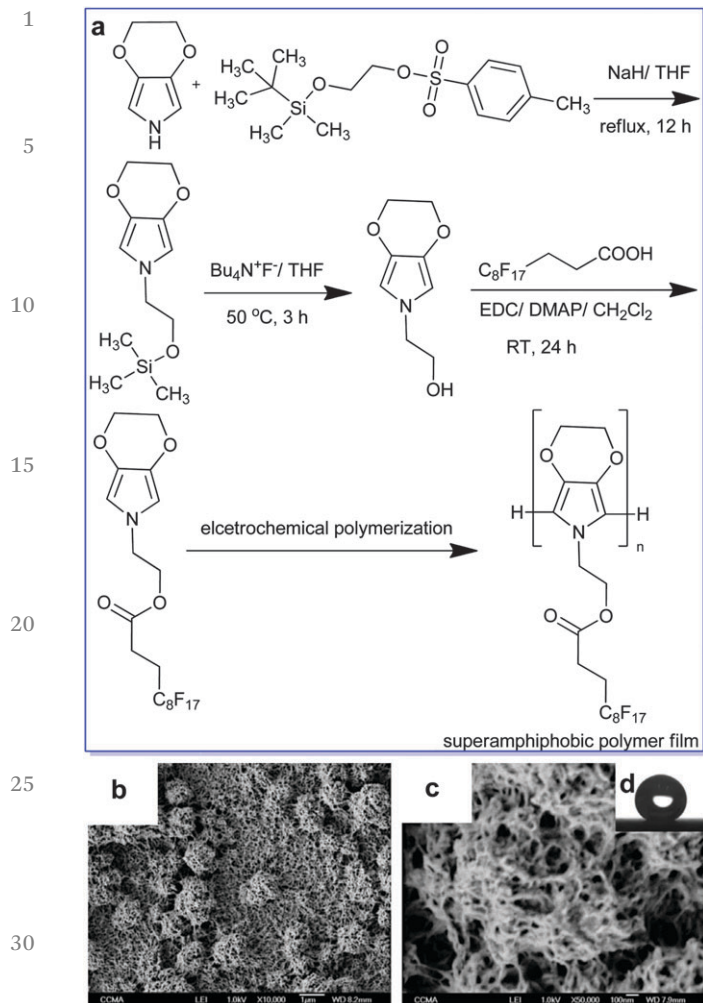
Jiang's group<sup>63</sup> developed a one-step electrodeposition process for the fabrication of superhydrophobic surfaces on a series of electrically conductive substrates such as copper, titanium, iron, zinc, aluminium, and tin, using *n*-tetradecanoic acid as an electrolyte. Hierarchical micro/nanostructures with excellent superhydrophobicity were obtained. Such coatings showed superhydrophobicity even for some corrosive liquids including salt solutions and acidic and basic solutions at all pH values. By replacing *n*-tetradecanoic acid with nonadecafluorodecanoic acid,<sup>63,64</sup> the authors were able to prepare superamphiphobic coatings with a microcluster of flower-like structures composed of nanosheets. The superamphiphobicity of the treated surface was attributed to the synergistic effect of their special surface compositions and textured structures. Compared with traditional approaches towards the preparation of superamphiphobic coatings, this one-pot method is much simpler and the procedure is more convenient to operate.

In Lin and coworkers' work,<sup>65</sup> electrically conductive superamphiphobic coatings were prepared *in situ* by one-step vapour-phase polymerisation of polypyrrole in the presence of a fluorinated alkyl silane on fibrous substrates. In a subsequent

work,<sup>66</sup> a robust, electrically conductive, superamphiphobic fabric was prepared by vapour-phase polymerisation of 3,4-ethylenedioxythiophene on fabric in the presence of FD-POSS and 1*H*,1*H*,2*H*,2*H*-perfluorooctyl triethoxysilane (FAS). The incorporation of FD-POSS and FAS into the polymeric layer improved the washing and abrasion stability considerably but had a very small influence on the conductivity. The coated fabric can withstand no less than 500 cycles of standard laundry and 10 000 cycles of the abrasion test without apparently changing its superamphiphobicity, though the conductivity showed a small reduction. Besides, the coating exhibited self-healing properties, *i.e.*, it auto-repairs its surface from chemical damage so as to restore its superamphiphobicity.

Saraf and coworkers<sup>67</sup> developed three different techniques to achieve superamphiphobicity using hydroentangled nylon non-woven fabrics as substrates: (1) pulsed plasma polymerization of 1*H*,1*H*,2*H*,2*H*-perfluorodecyl acrylate; (2) microwave-assisted condensation of 1*H*,1*H*,2*H*,2*H*-perfluorodecyltrimethoxysilane (FS); and (3) FS condensation through wet processing. The coated nonwoven fabrics showed very high  $\theta_{CA}$  for both water ( $\theta_{CA} = 168\text{--}174^\circ$ ) and dodecane ( $\theta_{CA} = 153\text{--}160^\circ$ ).

Darmanin and Guittard<sup>68</sup> prepared superamphiphobic nanoporous films by electrochemically polymerizing a fluorinated monomer 2-(2,3-dihydro-[1,4]dioxino[2,3-*c*]pyrrol-6-yl)ethyl 1*H*,1*H*,2*H*,2*H*-perfluorodecanoate, which was synthesized from 3,4-ethylenedioxyppyrole *via* a multi-step procedure (Fig. 10a). The electrochemical polymerization of the monomer was carried out by cyclic voltammetry using a solution of a mixture of monomer-tetrabutylammonium hexafluorophosphate in anhydrous acetonitrile. Polymerization was initiated on the surface of the platinum disk electrode by repeated potential scans between 1.00 V and 0.83 V, inducing a homogenous growth of an electroactive polymer film on the electrode. Then the polymers were very quickly deposited on gold at a constant potential and deposition charge.  $\theta_{CA}$  measurements indicated that the polymeric surfaces are both superhydrophobic ( $\theta_{CA} = 161^\circ$  for water) and superoleophobic ( $\theta_{CA} = 145^\circ$  for hexadecane, Fig. 10d). SEM images revealed that the surface morphology consists of a very porous material at a nanometric scale and an assembly of spherical structures at a micrometric scale (Fig. 10b and c). This two-scale construction enables the surface with exceptional super-antiwetting properties because it allows the surface to trap air beneath the surface, which supports the weight of a water–oil droplet more easily. In their subsequent studies,<sup>69,70</sup> the authors found that the length of the alkylendioxy bridge of the fluorinated 3,4-alkylenedioxyppyrole monomer plays a considerably important role in the surface morphology of the electrodeposited conducting polymer film: the polymerization of the fluorinated 3,4-ethylenedioxyppyrole monomer imparts the polymeric film with superamphiphobicity with extremely low CAH, whereas the polymerization of the fluorinated 3,4-propylenedioxyppyrole monomer gives only superhydrophobic films with sticking property ( $\theta_{SA} > 90^\circ$ ). The different wettability was attributed to the presence of nanoporosity in fluorinated poly(3,4-ethylenedioxyppyrole) films, which increases both oil and water  $\theta_{CA}$  and switches the system from the Wenzel to the Cassie–Baxter



**Q5** Fig. 10 Synthesis (a) and SEM images (b and c) of the polymeric surface, and a photo of a hexadecane droplet on the surface (d). The scale bar represents 1  $\mu\text{m}$  (b) and 100 nm (c), respectively. Reproduced with permission from ref. 68, Copyright 2009 by Academic Press.

state. Very recently, the same group has found that the surface microstructuration increases with the fluorinated-alkyl chain length, whereas the surface nanoporosity goes the reverse way.<sup>71</sup>

## 4. Functional applications

With the increasing demand for functional materials with excellent anti-wetting ability, a great deal of interest has been focused on the development of superamphiphobic surfaces displaying a wide range of applications.<sup>5,9</sup> The discussion below will focus on how surface superamphiphobic modification brings about new functions such as super-antiwetting, self-cleaning, anti-freezing, anti-bacterial activity, corrosion resistance, and oil droplets manipulation, to name but a few, which are not available for the materials themselves.

### 4.1. Super-antiwetting

There is no doubt that most applications of superamphiphobic surfaces are based on their versatile function in super-

antiwetting, and all the other applications are derived from such a basic function. Superamphiphobic surfaces display characteristics of both superhydrophobic and superoleophobic, and thereby they share most of the functions with superhydrophobic surfaces with some exceptions. For instance, superhydrophobic surfaces can normally be used for oil-water separation because these super-water-repellant surfaces are wettable by low surface tension oils;<sup>7</sup> however, it is obvious that superamphiphobic surfaces cannot be used in such an application. However, compared with superhydrophobic surfaces, the biggest advantage of superamphiphobic surfaces is their super-antiwetting ability not only for pure water but also for low surface tension aqueous solution (for *e.g.*, detergent solution, rain water, underground water, waste water, and sea water) and organic 'oils' (for *e.g.*, hexane, hexadecane, toluene, mineral oil, and cooking oil).<sup>9</sup>

In Seeger's group, superamphiphobic coatings with super-antiwetting ability for both water and various low-surface tension organic liquids were prepared using silicone nanofilaments through a grow-from approach.<sup>9</sup> As mentioned above (Section 3.1.1.1), with such a technique, a layer of SNF can be grown on various substrates by chemical deposition of trichloromethylsilane (TCMS) in the presence of water. The coated glass surfaces display super-antiwetting ability for probing liquid of water ( $\theta_{\text{CA}} = 168^\circ$ ,  $\theta_{\text{SA}} = 5^\circ$ ), but not for low-surface-tension 'oils'.<sup>9</sup> For example,  $\theta_{\text{CA}}$  of diiodomethane which shows a surface tension of  $50.8 \text{ mN m}^{-1}$  is  $91^\circ$ ; other 'oils' such as mineral oil, toluene, cyclohexane, hexadecane and decane which exhibit surface tension between  $32 \text{ mN m}^{-1}$  and  $23 \text{ mN m}^{-1}$  can spread on the surface quickly ( $\theta_{\text{CA}} \approx 0^\circ$ ), indicating that these samples are superoleophilic. Such coatings (on textile substrates) can be used for oil-water separation due to their superhydrophobicity not superoleophilicity.<sup>72</sup> Upon activating by  $\text{O}_2$  plasma and surface modifying with PFDTS, the coatings show superamphiphobicity and cannot be wetted by both water and low surface tension 'oils' (Fig. 11a). For all of the liquids mentioned above, a high  $\theta_{\text{CA}}$  ( $>155^\circ$ ) and low  $\theta_{\text{SA}}$  ( $<6^\circ$ ) on the coated glass surface were observed, indicating that all of the liquid droplets on such a surface are in the Cassie-Baxter state. The liquid droplets could easily roll off from the surface while it is slightly tilted ( $<6^\circ$ ). Even jets of toluene and decane could bounce off the TCMS-PFDTS coated surface without leaving a trace (Fig. 11b). The TCMS-PFDTS-coated glass surface was reflective in toluene and remained completely dry after taken out (Fig. 11c), implying the existence of an air cushion between the solid surface and the liquids. This means that most of the area beneath the liquid droplet is a liquid-vapour interface, and thereby the interaction between the liquid and the coating is extremely weak. Compared with superhydrophobic surfaces, superamphiphobic surfaces are more useful in antiwetting for practical applications since the former surfaces can be easily contaminated by oily substances when the surfaces are exposed to an industrial or household environment and gradually lose their superhydrophobicity, while the latter surfaces cannot be contaminated (Fig. 11) and their superamphiphobicity can be maintained for a long time.

The super-antiwetting function can be applied to many traditional materials such as glass,<sup>9,25,46,56</sup> silicon,<sup>5,7,42,43,55</sup>

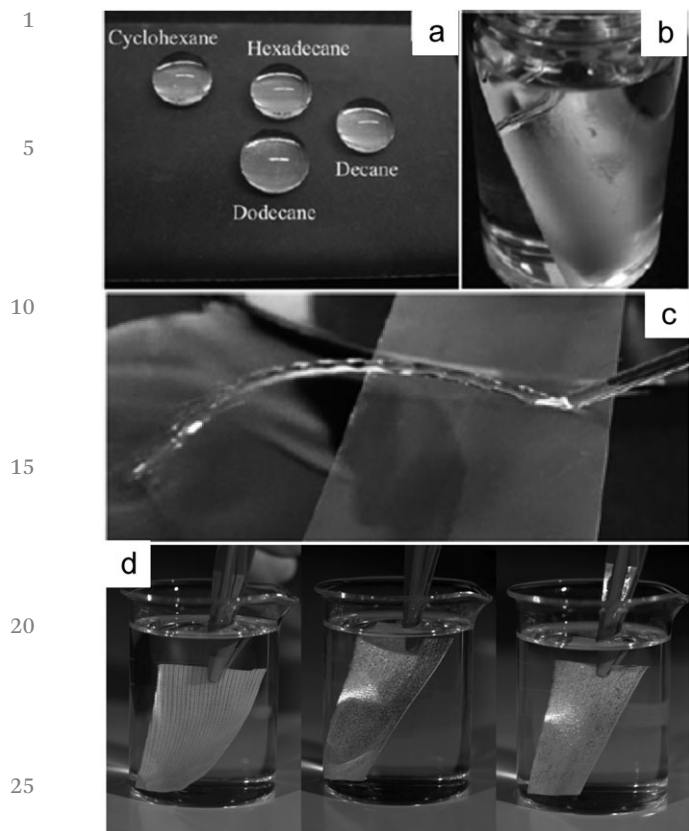


**Fig. 11** Images of the superamphiphobic glass slides with droplets of various non-polar liquids (a), immersed in toluene (b), and with a jet of toluene bouncing off (c), and (d) untreated polyester fabric immersed in hexadecane (left), a superamphiphobic fabric immersed in hexadecane (middle) and heptane (right). (a–c) Reproduced from ref. 9, Copyright Wiley 2011. (d) Reproduced from ref. Reprinted with permission from ref. 53, Copyright Elsevier 2012.

zinc,<sup>6,50</sup> aluminium,<sup>6,33</sup> iron,<sup>6</sup> steel,<sup>60</sup> copper,<sup>34,63</sup> nickel,<sup>6</sup> engineering metal alloys,<sup>6</sup> textile,<sup>23,53</sup> polyester fabric,<sup>61</sup> paper,<sup>62</sup> gel,<sup>51,52</sup> and so on, protecting their surfaces from being wetted, contaminated or fouled by water and oil pollutants. Besides, the superamphiphobic surface modification brings about not only the super-antiwetting function but also other derived functions such as self-cleaning, anti-fogging, anti-bacterial activity, corrosion resistance, and oil transportation, which will be discussed in the following sections.

#### 4.2. Self-cleaning

Self-cleaning coatings can be broadly classified into two major types: photocatalysis-induced superhydrophilic coatings and superhydrophobic or superamphiphobic coatings.<sup>47</sup> In superhydrophilic coatings ( $\theta_{CA} < 5^\circ$ ), the surface is cleaned by the sheeting effect of water and also by breaking down the complex organic substances into carbon dioxide and water—the photocatalytic effect. In contrast, in superhydrophobic or superamphiphobic surfaces, the air pockets that get trapped between the nanostructured substrate and the water droplet result in the formation of a composite solid/air/liquid interface, which leads

to an increase in  $\theta_{CA}$  of the liquid droplet, thereby facilitating the de-wetting of the surface and enabling the droplet to roll-off easily, taking away the dirt and other pollutants.<sup>46,47</sup>

#### 4.3. Anti-freezing

Anti-freezing on the material surface has long been a technological challenge because some outdoor infrastructures and high-technological devices such as aviation, space flight and radar can be easily affected or even destroyed by the large amount of adherent ice. For instance, supercooled water vapour and clouds in the upper-air layers can easily condense and subsequently freeze on aircraft surfaces during a flight, which results in the worst case in a dramatic decrease of the ascending force and may lead to an airplane's crash, e.g., on October 31, 1994, when American Eagle Flight 4184 crashed because of ice formation on the wings after flying in icing conditions.

Surface superhydrophobic modification shows great potential to address such a challenge. Quéré *et al.*<sup>73</sup> demonstrated that freezing could remarkably be delayed when water droplets were deposited on cold superhydrophobic surfaces. It was reported that the presence of microtextures dramatically delay the freezing time of the water drops, by a factor between 3 and 5. Water droplets rolled off the cold superhydrophobic surface quickly without freezing. In contrast, drops on an untreated surface spread quickly and formed a thin film on the surface, which was frozen immediately. The authors pointed out that the air sublayer in a superhydrophobic surface could provide substantial thermal insulation and thus delayed the freezing process. In the work by Song *et al.*,<sup>74</sup> it was observed that the presence of micro/nanostructural and chemical patterns is very important for the controlling of coalescence of microdroplets as well as their quick self-removal. Kulinich and Farzaneh<sup>75</sup> discovered that CAH plays an important role in anti-freezing and a lower CAH normally contributes to a much longer delay of freezing time.<sup>73,75</sup>

Compared with superhydrophobic surfaces, superamphiphobic surfaces normally exhibit much lower water CAH ( $\theta_{SA}$  close to  $1^\circ$  or even lower), as documented extensively.<sup>9,25,46,47,60</sup> Therefore, superamphiphobic surfaces are more promising in anti-freezing though the corresponding study in such an application for superamphiphobic surfaces has not yet been reported.

#### 4.4. Anti-bacterial growth properties

In addition to extreme non-wettability, superamphiphobic surfaces also exhibit antibacterial activity.<sup>76–78</sup> Vilčnik *et al.*<sup>76,77</sup> investigated the antibacterial properties of hydrophobic–oleophobic sol–gel coatings for cotton fabrics by using *Escherichia coli* bacteria as a model, and found that superamphiphobic surfaces exhibited a long lasting antibacterial effect without the addition of any antibacterial agents. The antibacterial activity test revealed that the reduction of the bacteria on superamphiphobic cotton fabrics was nearly 100%.<sup>77</sup> In Huang's group,<sup>78</sup> superamphiphobic cellulose (commercial filter paper) was fabricated by chemical etching using alkaline solution to enhance the surface roughness, followed by depositing ultrathin titania films *via* a facile surface sol–gel process, and subsequently surface modifying using 1*H*,1*H*,2*H*,2*H*-perfluorooctyl trimethoxysilane

1 (PFOTMS). Due to the combined surface roughness and low  
2 surface energy of the PFOTMS monolayers, the naturally hydro-  
3 philic filter paper was converted into superamphiphobic, which  
4 effectively inhibited the adhesion of bacteria such as lysogenic  
5 *Escherichia coli*.

#### 4.5. Corrosion resistance

6 The oxidation and corrosion of metals and their alloys in the  
7 humid atmosphere limit their applications, causing serious  
8 problems such as accelerated aging of the devices, huge waste,  
9 and environmental contamination.<sup>79</sup> Surface superamphipho-  
10 bic modification is a probable solution to these problems  
11 because the super-repellant coating acts as durable barrier film  
12 that can effectively prevent the metal surface from being  
13 corroded. Recently, a superamphiphobic CaLi-based bulk  
14 metallic glass,<sup>41</sup> which was prepared by the construction  
15 of micro/nanoscale hierarchical structures and subsequent  
16 fluorination, was reported to show long-term stable anti-  
17 corrosion ability due to its durable superamphiphobicity that  
18 can be kept under ambient atmospheric conditions for more  
19 than three months. In Jiang's group,<sup>8,63</sup> engineering metals and  
20 their alloys such as zinc, aluminium, iron, nickel and Zn-Fe  
21 alloy are superamphiphobic-functionalized by taking advantage  
22 of an electrochemical reaction in perfluorocarboxylic acid  
23 solution, which shows great promise in corrosion resistance  
24 for real applications since these metals are the most important  
25 and applicable materials in industry. In the work performed by  
26 Zhang *et al.*,<sup>33</sup> superamphiphobic aluminium was prepared in a  
27 facile way of HCl etching, followed by PFOA surface modifica-  
28 tion. In another study by the same research group,<sup>80</sup> super-  
29 amphiphobic copper sheets were fabricated *via* a simple and  
30 time-saving procedure: sandblasting and Ag deposition processes  
31 were used to create surface roughness firstly, and then the resultant  
32 surfaces were fluorinated by simply immersing the samples in  
33 PFDSH-ethanol solution (1 mM) for only 30 s. The obtained  
34 superamphiphobic surfaces exhibited enhanced corrosion  
35 resistance with a more positive corrosion potential and a more  
36 negative corrosion current density. More interestingly, the  
37 superamphiphobicity could be restored by a simple regenera-  
38 tion process when loss of superoleophobicity occurred. The  
39 authors suggested that such a simple and time-saving fabrica-  
40 tion technique will make it possible for large-scale production  
41 of superamphiphobic engineering materials. Very recently,  
42 Tuteja and coworkers<sup>60</sup> developed superamphiphobic stainless  
43 steel wire meshes by electrospinning a blend of cross-linked  
44 poly(dimethylsiloxane) and FD-POSS. It was observed that the  
45 coated steel surface cannot be corroded by concentrated hydro-  
46 chloric acid and concentrated sodium hydroxide.

#### 4.6. Oil droplets manipulation

47 Recently, utilizing superamphiphobic surfaces with controllable  
48 oil adhesion, Jiang and coworkers constructed an oil droplet-  
49 based microreactor for oil droplets manipulation.<sup>35</sup> The surface  
50 adhesion to oil can be tuned through the adjustment of either  
51 surface nanostructures or external preload forces, making it  
52 possible for oil transportation in a drop-to-drop system. In their

53 experiment, an oil droplet containing a styrene monomer was  
54 transferred from a low adhesive superamphiphobic surface to a  
55 metal cap, which was then reacted with another oil droplet  
56 containing Br<sub>2</sub> on a high adhesion superamphiphobic surface.  
57 After the reaction of the two droplets, the final droplet was left  
58 on the substrate due to its high adhesion to the surface. These  
59 surfaces with controllable oil adhesion displayed promising  
60 applications in microfluidic systems, no-loss oil droplet trans-  
61 portation, and other fields.

#### 4.7. Other applications

62 Except the functional applications discussed above, super-  
63 amphiphobic surfaces also exhibit great potential in a variety of  
64 other fields including breathable protective wear,<sup>23</sup> enhanced  
65 solvent resistance,<sup>9</sup> chemical shielding,<sup>60</sup> drag reduction,<sup>81</sup>  
66 patterned superfunctional surfaces,<sup>15</sup> smart devices,<sup>51</sup> anti-  
67 reflection, and oil capture.

## 5. Conclusions and perspectives

68 This review summarizes the characterization, fabrication, and  
69 functional applications of superamphiphobic surfaces. The  
70 development of such surfaces is important for basic research,  
71 as well as, for numerous commercial applications. Through  
72 years of endless efforts, great achievements have been made in  
73 this field: a variety of different techniques towards the fabrica-  
74 tion of superamphiphobic surfaces have been developed  
75 by combining the design of surface roughness and surface  
76 chemistry. Nevertheless, there are still lots of challenges that  
77 need to be addressed. For example, a majority of the fabrication  
78 methods are limited to laboratory research and not suitable  
79 for industrial scale production. Even though the superamphi-  
80 phobic coatings can be prepared on a large scale, they generally  
81 face the problem of poor mechanical stability. Mechanical  
82 durability is crucial to practical applications, *i.e.*, they cannot  
83 find practical use without sufficient mechanical stability. How-  
84 ever, this aspect has been sparingly addressed in the literature  
85 and there is a need and an opportunity to develop mechanically  
86 durable superamphiphobic surfaces. The relationship between  
87 mechanical stability and surface morphology as well as surface  
88 chemistry needs to be investigated. Quantitative ways to char-  
89 acterize the mechanical stability of superamphiphobic coat-  
90 ings should be established—probably there would be a critical  
91 force above which the superamphiphobicity of the surface  
92 decreases substantially and methods for precise determination  
93 of such a critical force need to be figured out.

94 Future trends in this field may see an expansion towards  
95 self-healing superamphiphobicity because it shows great  
96 promise in practical applications—their oil-repellency can  
97 easily be automatically restored after mechanical damage.  
98 Surfaces with controllable superamphiphobicity may also  
99 become one of the focuses of future research, given the  
100 biological relevance of most of them.

101 Overall, we believe that an exciting future for superamphi-  
102 phobic surfaces will be witnessed since many scientists and

1 engineers contribute to the understanding and the design of  
2 such surfaces.

## 5 Acknowledgements

Financial support from University of Zurich and Swiss National  
Science Foundation (SNSF) is greatly acknowledged.

## 10 Notes and references

- 1 H. Ollivier, *Ann. Chim. Phys.*, 1907, **10**, 229–288.
- 2 W. Barthlott and C. Neihuis, *Planta*, 1997, **202**, 1–8.
- 3 X. Zhang, F. Shi, J. Niu, Y. Jiang and Z. Wang, *J. Mater.*  
15 *Chem.*, 2008, **18**, 621–633, and references therein.
- 4 M. Liu, Y. Zheng, J. Zhai and L. Jiang, *Acc. Chem. Res.*, 2010,  
**43**, 368–377.
- 5 A. Tuteja, W. Choi, M. L. Ma, J. M. Mabry, S. A. Mazzella,  
G. C. Rutledge, G. H. McKinley and R. E. Cohen, *Science*,  
20 **2007**, **318**, 1618–1622.
- 6 H. F. Meng, S. T. Wang, J. M. Xi, Z. Y. Tang and L. Jiang,  
*J. Phys. Chem. C*, 2008, **112**, 11454–11458.
- 7 A. Tuteja, W. Choi, J. M. Mabry, G. H. McKinley and  
R. E. Cohen, *Proc. Natl. Acad. Sci. U. S. A.*, 2008, **105**,  
25 18200–18205.
- 8 T. Darmanin and Guittard, *Langmuir*, 2009, **25**, 5463–5466.
- 9 J. Zhang and S. Seeger, *Angew. Chem., Int. Ed.*, 2011, **50**,  
6652–6656.
- 10 H.-J. Butt, C. Semprebon, P. Papadopoulos, D. Vollmer,  
M. Brinkmann and M. Ciccotti, *Soft Matter*, 2013, **9**,  
30 418–428.
- 11 J. Genzer and K. Efimenko, *Biofouling*, 2006, **22**, 339–360.
- 12 R. N. Wenzel, *Ind. Eng. Chem.*, 1936, **28**, 988–994.
- 13 A. B. D. Cassie and S. Baxter, *Trans. Faraday Soc.*, 1944, **40**,  
35 546–551.
- 14 J. Zimmermann, S. Seeger and F. A. Reifler, *Text. Res. J.*,  
2009, **79**, 1565–1570.
- 15 J. Zimmermann, M. Rabe, G. R. J. Artus and S. Seeger, *Soft*  
*Matter*, 2008, **4**, 450–452.
- 16 L. Cao, T. P. Price, M. Weiss and D. Gao, *Langmuir*, 2008, **24**,  
40 1640–1643.
- 17 H. J. Li, X. B. Wang, Y. L. Song, Y. Q. Liu, Q. S. Li, L. Jiang  
and D. B. Zhu, *Angew. Chem., Int. Ed.*, 2001, **40**, 1743–1746.
- 18 K.-H. Cho and L.-J. Chen, *Nanotechnology*, 2011, **22**, 445706,  
45 and references therein.
- 19 G. R. J. Artus, S. Jung, J. Zimmermann, H.-P. Gautschi,  
K. Marquardt and S. Seeger, *Adv. Mater.*, 2006, **18**, 2725–2762.
- 20 T.-S. Wong, S. H. Kang, S. K. Y. Tang, E. J. Smythe,  
B. D. Hatton, A. Grinthal and J. Aiyenberg, *Nature*, 2011,  
477, 443–447.
- 21 Y. Huang, J. Zhou, B. Su, L. Shi, J. Wang, S. Chen, L. Wang,  
J. Zi, Y. Song and L. Jiang, *J. Am. Chem. Soc.*, 2012, **134**,  
17053–17058.
- 22 M. Kuang, J. Wang, B. Bao, F. Li, L. Wang, L. Jiang and  
47 **Q7** Y. Song, *Adv. Opt. Mater.*, 2014, DOI: 10.1002/  
adom.201300369.
- 23 B. Leng, Z. Shao, G. de With and W. Ming, *Langmuir*, 2009,  
**25**, 2456–2460.
- 24 C.-T. Hsieh, F.-L. Wu and W.-Y. Chen, *Mater. Chem. Phys.*,  
2010, **121**, 14–21.
- 25 Z. He, M. Ma, X. Lan, F. Chen, K. Wang, H. Deng, Q. Zhang  
and Q. Fu, *Soft Matter*, 2011, **7**, 6435–6443.
- 26 C.-F. Wang, W.-Y. Chen, H.-Z. Cheng and S.-L. Fu, *J. Phys.*  
*Chem. C*, 2010, **114**, 15607–15611, and references therein.
- 27 M. Zhang, T. Zhang and T. Cui, *Langmuir*, 2011, **27**,  
9295–9301.
- 28 A. Das, T. M. Schutzius, I. S. Bayer and C. M. Megaridis,  
*Carbon*, 2012, **50**, 1346–1354.
- 29 J. Zimmermann, S. Seeger, G. Artus and S. Jung, *WO Pat.*,  
2004113456, 2004.
- 30 J. Zimmermann, F. A. Reifler, G. Fortunato, L.-C. Gerhardt  
and S. Seeger, *Adv. Funct. Mater.*, 2008, **18**, 3662–3669.
- 31 J. Zimmermann, G. R. J. Artus and S. Seeger, *Appl. Surf. Sci.*,  
2007, **253**, 5972–5979.
- 32 J. Zimmermann, F. A. Reifler, U. Schrade, G. R. J. Artus and  
S. Seeger, *Colloids Surf., A*, 2007, **302**, 234–240.
- 33 J. Yang, Z. Zhang, X. Xu, X. Men, X. Zhu and X. Zhou, *New*  
*J. Chem.*, 2011, **35**, 2422–2426.
- 34 X. Zhu, Z. Zhang, X. Xu, X. Mena, J. Yang, X. Zhou and  
Q. Xue, *J. Colloid Interface Sci.*, 2012, **367**, 443–449.
- 35 X. Yao, Y. Song and L. Jiang, *Adv. Funct. Mater.*, 2011, **21**,  
25 4270–4276.
- 36 H. Kim, K. Noh, C. Choi, J. Khamwannah, D. Villwock and  
S. Jin, *Langmuir*, 2011, **27**, 10191–10196.
- 37 L. Cao, T. P. Price, M. Weiss and D. Gao, *Langmuir*, 2008, **24**,  
30 1640–1643.
- 38 Y. Liu, Y. Xiu, D. W. Hess and C. P. Wong, *Langmuir*, 2010,  
**26**, 8908–8913.
- 39 S. M. Ramos, A. Benyagoub, B. Canut and C. Jamois,  
*Langmuir*, 2010, **26**, 5141–5146.
- 40 C. Aulin, S. H. Yun, L. Wågber and T. Lindström, *ACS Appl.*  
35 *Mater. Interfaces*, 2009, **1**, 2443–2452.
- 41 K. Zhao, K. S. Liu, J. F. Li, W. H. Wang and L. Jiang, *Scr.*  
*Mater.*, 2009, **60**, 225–227.
- 42 H. Zhao, K.-Y. Law and V. Sambhy, *Langmuir*, 2011, **27**,  
5927–5935.
- 43 H. Zhao and K.-Y. Law, *Langmuir*, 2012, **28**, 11821–11827.
- 44 M. Im, H. Im, J.-H. Lee, J.-B. Yoon and Y.-K. Choi, *Soft*  
*Matter*, 2010, **6**, 1401–1404.
- 45 A. Susarrey-Arce, Á. G. Marín, L. Lefferts, J. G. E. Gardeniers  
and A. von Houselt, *J. Micromech. Microeng.*, 2013, **23**, 025004.
- 46 X. Deng, L. Mannen, H.-J. Butt and D. Vollmer, *Science*,  
2012, **335**, 67–70.
- 47 V. A. Ganesh, S. S. Dinachali, H. K. Raut, T. M. Walsh,  
A. S. Nair and S. Ramakrishna, *RSC Adv.*, 2013, **3**,  
3819–3824.
- 48 T. Fujii, Y. Aoki and H. Habazaki, *Langmuir*, 2011, **27**,  
11752–11756.
- 49 T. Fujii, H. Sato, E. Tsuji, Y. Aoki and H. Habazaki, *J. Phys.*  
*Chem. C*, 2012, **116**, 23308–23314.
- 50 X. Xu, Z. Zhang, F. Guo, J. Yang, X. Zhu, X. Zhou and Q. Xue,  
55 *Colloids Surf., A*, 2012, **396**, 90–95.

- 1 51 H. Jin, M. Kettunen, A. Laiho, H. Pynnönen, J. Paltakari, A. Marmur, O. Ikkala and R. H. A. Ras, *Langmuir*, 2011, **27**, 1930–1934.
- 52 H. Jin, X. Tian, O. Ikkala and R. H. A. Ras, *ACS Appl. Mater. Interfaces*, 2013, **5**, 485–488.
- 53 G. R. J. Artus, J. Zimmermann, F. A. Reifler, S. A. Brewer and S. Seeger, *Appl. Surf. Sci.*, 2012, **258**, 3835–3840.
- 54 Y.-C. Sheen, Y.-C. Huang, C.-S. Liao, H.-Y. Chou and F.-C. Chang, *J. Polym. Sci., Part B: Polym. Phys.*, 2008, **46**, 1984–1990.
- 10 55 R. Campos, A. J. Guenther, A. J. Meuler, A. Tuteja, R. E. Cohen, G. H. McKinley, T. S. Haddad and J. M. Mabry, *Langmuir*, 2012, **28**, 9834–9841.
- 56 X. Wang, H. Hu, Q. Ye, T. Gao, F. Zhou and Q. Xue, *J. Mater. Chem.*, 2012, **22**, 9624–9631.
- 15 57 J. Yang, Z. Zhang, X. Men, X. Xu and X. Zhu, *New J. Chem.*, 2011, **35**, 576–580.
- 58 D. Han and A. J. Steckl, *Langmuir*, 2009, **25**, 9454–9462.
- 59 S. Srinivasan, S. S. Chhatre, J. M. Mabry and R. E. Cohen, *Polymer*, 2011, **52**, 3209–3218.
- 20 60 S. Pan, A. K. Kota, J. M. Mabry and A. Tuteja, *J. Am. Chem. Soc.*, 2013, **135**, 578–581.
- 61 H. Wang, Y. Xue, J. Deng, L. Feng, X. Wang and T. Lin, *Angew. Chem., Int. Ed.*, 2011, **50**, 11433–11436.
- 25 62 D. Xiong, G. Liu and L. Hong, *Chem. Mater.*, 2011, **23**, 4357–4366.
- 63 J. Xi, L. Feng and L. Jiang, *Appl. Phys. Lett.*, 2008, **92**, 053102.
- 64 H. Meng, S. Wang, J. Xi, Z. Tang and L. Jiang, *J. Phys. Chem. C*, 2008, **112**, 11451–11458.
- 30 65 H. Wang, Y. Xue and T. Lin, *Soft Matter*, 2011, **7**, 8158–8161.
- 66 H. Wang, H. Zhou, A. Gestos, J. Fang, H. Niu, J. Ding and T. Lin, *Soft Matter*, 2013, **9**, 277–282.
- 67 R. Saraf, H. J. Lee, S. Michielsen, J. Owens, C. Willis, C. Stone and E. Wiluzs, *J. Mater. Sci.*, 2011, **46**, 5751–5760.
- 68 T. Darmanin and F. Guittard, *J. Colloid Interface Sci.*, 2009, **335**, 146–149.
- 69 T. Darmanin and F. Guittard, *Chem. Commun.*, 2009, 2210–2211.
- 70 T. Darmanin and F. Guittard, *J. Am. Chem. Soc.*, 2009, **131**, 7928–7933.
- 71 H. Bellanger, T. Darmanin and F. Guittard, *Langmuir*, 2012, **28**, 186–192.
- 72 J. Zhang and S. Seeger, *Adv. Funct. Mater.*, 2011, **21**, 4699–4704.
- 73 P. Tourkine, M. Le Merrer and D. Quéré, *Langmuir*, 2009, **25**, 7214–7216.
- 74 M. He, Q. Zhang, X. Zeng, D. Cui, J. Chen, H. Li, J. Wang and Y. Song, *Adv. Mater.*, 2013, **25**, 2291–2295.
- 75 S. A. Kulinich and M. Farzaneh, *Appl. Surf. Sci.*, 2009, **255**, 8153–8157.
- 76 B. Tomšič, B. Simončič, B. Orel, L. Černe, P. F. Tavčer, M. Zorko, I. Jerman, A. Vilčnik and J. Kovač, *J. Sol-Gel Sci. Technol.*, 2008, **47**, 44–57.
- 77 A. Vilčnik, I. Jerman, A. S. Vuk, M. Koželj, B. Orel, B. Tomšič, B. Simončič and J. Kovač, *Langmuir*, 2009, **25**, 5869–5880.
- 78 C. Jin, Y. Jiang, T. Niu and J. Huang, *J. Mater. Chem.*, 2012, **22**, 12562–12567.
- 79 X. Yao, Y. Song and L. Jiang, *Adv. Mater.*, 2011, **23**, 719–734.
- 80 Z. Zhang, X. Zhu, J. Yang, X. Xu, X. Meng and Z. Zhou, *Appl. Phys. A: Mater. Sci. Process.*, 2012, **108**, 601–606.
- 81 C. Lee and C.-J. Kim, *Phys. Rev. Lett.*, 2011, **106**, 014502.

35

35

40

40

45

45

50

50

55

55